The heart of oxygenic photosynthesis illuminated

Janssen, G.J.

Citation
Janssen, G. J. (2013, December 4). *The heart of oxygenic photosynthesis illuminated*. Retrieved from https://hdl.handle.net/1887/22697

Version:	Not Applicable (or Unknown)
License:	Leiden University Non-exclusive license
Downloaded from:	https://hdl.handle.net/1887/22697

Note: To cite this publication please use the final published version (if applicable).

Cover Page

Universiteit Leiden

The handle http://hdl.handle.net/1887/22697 holds various files of this Leiden University dissertation.

Author: Janssen, Geertje Jacoba
Title: The heart of oxygenic photosynthesis illuminated
Issue Date: 2013-12-04

Chapter 5

Time-resolved photo-CIDNP MAS NMR on PSI and PSII from plants

Excitation of the electronic states of photosynthetic RCs by nanosecond laser flashes allows for the visualization of transient polarization and provides insight into the mechanisms behind the buildup of polarization during repeated photo-cycles (Daviso *et al.* 2009). ns-flash photo-CIDNP MAS NMR can be applied to study the mechanism of photo-CIDNP buildup and the electronic structure of the active cofactors in PSI and PSII prior to spin diffusion. Up to this point, time-resolved photo-CIDNP MAS NMR experiments were restricted to bacterial systems (Daviso 2008; Daviso *et al*. 2009 and 2010b). In this chapter the first time-resolved photo-CIDNP data sets obtained from plant photosystems will be presented. ns-flash Photo-CIDNP has been applied to uniformly ^{15}N and selectively 4-ALA ^{13}C labeled PSI-110 particles. The experimental results and quantum chemical calculations suggest that the DD mechanism is the dominant mechanism in photo-CIDNP buildup in PSI and that mainly P_B acts as the electron donor. The results are in agreement with bidirectional electron transfer and the observed kinetics provides evidence for a high functional flexibility of PSI. In addition, this chapter discusses time-resolved photo-CIDNP data collected from D1D2 PSII particles of spinach. The results show that photo-CIDNP buildup in PSII resembles the buildup observed for *Rb. sphaeroides* R26 RCs. This can be explained by the relatively long lifetime of the triplet state in PSII and R26, which contrasts with the long triplet lifetime for WT *Rb. sphaeroides* bacterial RCs and PSI.

5.1 INTRODUCTION

5.1.1 Electron-Spin Echo Signals and Time-resolved Photo-CIDNP

In time-resolved photo-CIDNP experiments, excitation of the electronic states of the photosynthetic RC is achieved though illumination with nanosecond laser flashes. Each laser flash has a duration, τ_p ~ 8 ns and is followed by a variable delay time Δt between the laser pulse and the start of the NMR $\pi/2$ detection pulse, which has a duration of ~ 5 μs. This finite pulse length determines the time resolution for the detection of the polarization established by the coherence transfer and decay kinetics in a time-resolved photo-CIDNP experiment.

The buildup of photo-CIDNP occurs on the nanosecond time scale by coherent mixing of nuclear states with the non-stationary electron zero quantum state generated by photoexcitation and charge separation, and is revealed by the subsequent chemical decay kinetics (Figure 5.1). When radical pairs produced by continuous illumination are kept together for ~100 ns, by impairing the electron transfer from the acceptor to the quinone and from the cytochrome or OEC into the donor, the electronic zero quantum coherence of the singlet radical pair is converted into T_0 double quantum coherence by the electron-nuclear hyperfine interactions in what is called nowadays a "quantum biology" process. Net nuclear polarization accumulates from three mechanisms that break the antisymmetry of the population of nuclear spin states, TSM, DD and DR. Both TSM and DD require hyperfine anisotropy. The fully coherent TSM polarization buildup in addition requires a nonzero magnitude of the pseudosecular contribution to the hyperfine interaction, $B = \sqrt{\left(A_{zx}^2 + A_{zy}^2\right)}$. The TSM mechanism is strongest when $2\left|d\right| = 2\left|\omega_I\right| = \left|A\right|$, while the DD mechanism has its maximum when $2\left|\omega_I\right| = \left|A\right|$ (Jeschke and Matysik 2003). In RCs with a long lived triplet donor the DR relaxation mechanism occurs in addition to the TSM and the DD (Jeschke and Matysik 2003). For the DR mechanism, nuclear polarization of the donor in its triplet state is rapidly and selectively depleted by longitudinal paramagnetic relaxation of nuclear polarization during the ^{3}DA triplet lifetime. This exposes the opposite polarization generated via the $^1(D^{+\bullet}A^{-\bullet})$ singlet and $^3(D^{+\bullet}A^{-\bullet})$ triplet decay pathways. In ns-flash photo-CIDNP MAS NMR experiments, the τ_p of the laser pulse used for excitation is shorter than the time scale of the electron-nuclear coherence transfer. This allows for the detection of the primary coherence transfer processes that drive the photo-CIDNP and visualization of the polarization buildup before it spreads into the system by nuclear spin diffusion and relaxes to thermal equilibrium (Daviso *et al.* 2008b). The transfer of nuclear polarization established by

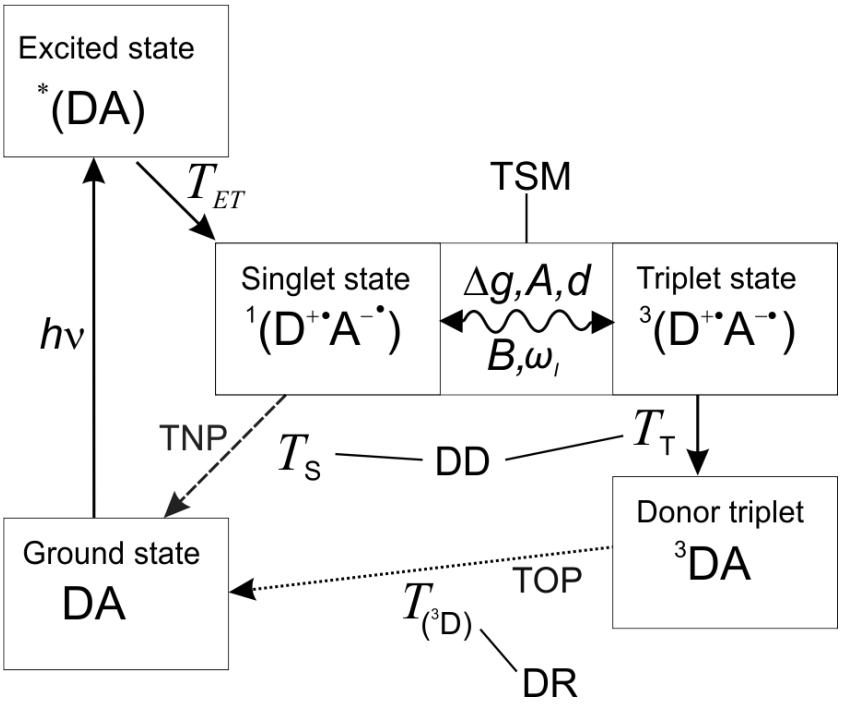

Figure 5.1: The electron-nuclear coherent mixing and chemical decay kinetics for the generation of photo-CIDNP in natural RCs at moderately high field, corresponding with 200-400 MHz ^{1}H NMR frequency. Three mechanisms are thought to be responsible for the buildup of net nuclear polarization in the solid-state, TSM, DD and DR. The evolution from the singlet state $^1(D^{+\bullet}A^{-\bullet})$ to the triplet state $^3(D^{+\bullet}A^{-\bullet})$ and back is accompanied by a transfer of fictitious electron polarization to the nuclei (Jeschke, 1997). In TSM net nuclear polarization is generated in the spin correlated radical pair due to the presence of both the pseudosecular part of the hyperfine interaction (*B*) and the coupling between the two electron spins (*d*), where the antisymmetry is broken in the presence of the nuclear Zeeman interaction (ω_I) in a fully coherent process. The TSM contribution is strongest at the matching condition $|A| \approx 2|d| \approx 2|\omega_I|$. In the DD mechanism, the formation of net nuclear polarization is based on different lifetimes for the singlet and the triplet radical pair states, T_S and T_T, respectively. In the DR, net nuclear polarization is thought to arise from opposite polarization in singlet and triplet radical pairs that do not cancel when part of the triplet-derived polarization relaxes during the triplet lifetime, $T_{(^3D)}$ (McDermott *et al.* 1998). This requires that the longitudinal relaxation time of the nuclei in the RC triplet is shortened to such an extent that it is comparable to $T_{(^3D)}$ (Jeschke and Matysik 2003; Daviso *et al.* 2007). The dashed arrow indicates the path of the transient nuclear polarization (TNP) generated in the singlet radical state and detected in the ground state. The dotted arrow indicates the path of the transiently obscured polarization (TOP) induced by the paramagnetic triplets. Nuclear polarization becomes observable when the excited triplet states decay to the ground state.

the photo-CIDNP effect by spin diffusion on the ms time scale was demonstrated in studies of ^{13}C ALA labeled RCs, with ^{13}C nuclei incorporated pairwise into the BChl cofactors. In addition, time-resolved photo-CIDNP experiments allow for the selective observation of nuclear polarization visualized through decay to the groundstate via the $^1(D^{+\bullet}A^{-\bullet})$ chemical species at $T_{(^3D)} > \Delta t > T_S$. As described earlier by Polenova and McDermott, the initial radical pair singlet is unpolarized and fully occupied at time, $t = T_{ET,}$ after which the molecular triplet species, ^{3}DA, and both singlet, $^1(D^{+\bullet}A^{-\bullet})$, and triplet, $^3(D^{+\bullet}A^{-\bullet})$, radical pair states get populated and polarized (Polenova and McDermott 1999). At $T_{(^3D)} > t > T_S$, the ground state is populated with a preference for a nuclear beta state due to the relative fast decay to the

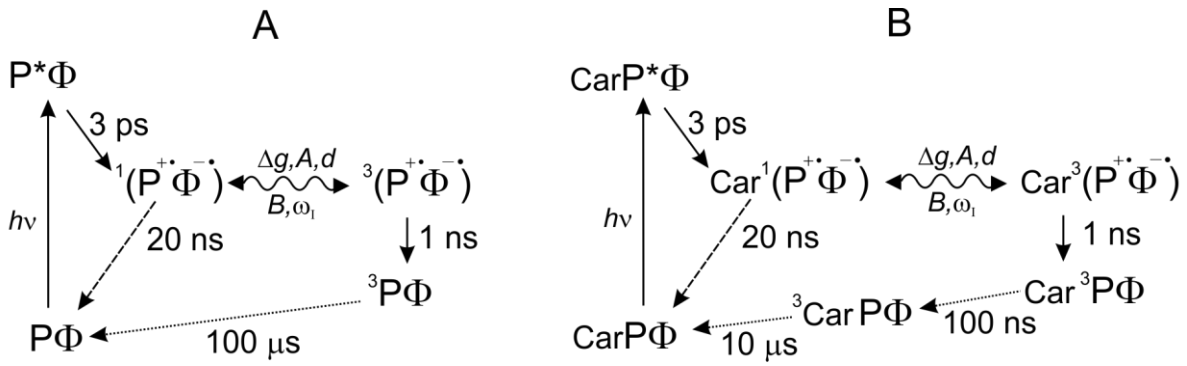

Figure 5.2: Kinetics and spin dynamics of electron transport for quinone-depleted RCs of the carotenoid-less strain R26 of *Rb. sphaeroides* (A) and for the corresponding wild type (B). After the absorption of a photon to produce the photochemically excited state of the primary donor P*, an electron is transferred to the primary acceptor Φ, a bacteriopheophytin cofactor. This leads to the initial singlet radical pair $^{1}(P^{+\bullet}\Phi^{-\bullet})$ in a non-stationary state, which can be represented as a polarized fictitious electron spin state (Jeschke 2008). Electron back transfer leads to the initial electronic ground state with a T_S of 20 ns. Due to hyperfine interaction with nuclei, the singlet radical pair coherently evolves into a triplet radical pair $^{3}(P^{+\bullet}\Phi^{-\bullet})$. Net nuclear polarization is produced by unbalancing the decay branches of the singlet and the triplet radical pair. (B) In *Rb. Spaeroides* WT the triplet donor ^{3}P is quenched by a nearby carotenoid, leading to a triplet excited state (^{3}Car) with a lifetime of ~10 μs. The dashed arrows indicate the path and timing of the transient nuclear polarization associated with the singlet radical state and detected in the ground state (Daviso 2008). The dotted arrows indicate path and timings of the transiently obscured polarization induced by paramagnetic triplets.

groundstate via the $^{1}(D^{+\bullet}A^{-\bullet})$ chemical species. From $t > T_{(^{3}D)}$ onward, all molecules are in the ground state and polarized (Polenova and McDermott 1999).

5.1.2 Photo-CIDNP buildup in bacterial RC

Time-resolved ns flash photo-CIDNP MAS NMR has been applied to bacterial RCs of *Rb. sphaeroides* WT and its carotenoid deficient mutant R26 to resolve the electronic structure of the primary electron donor and establish the mechanism of photo-CIDNP buildup (Daviso 2008; Daviso *et al*. 2009 and 2010b). Figure 5.2 summarizes the essentials of the decay kinetics and coherent spin dynamics. In WT RCs the Car is within van der Waals distance of the special pair. This leads to rapid quenching of the triplet donor via the formation of an excited ^{3}Car triplet state with a lifetime of ~10 μs. For the WT initially weak positive donor signals are observed due to the excess of nuclear polarization generated through decay to the groundstate via the singlet radical state before (see Figure 5.2 and Daviso *et al.* 2009). The initial rapid phase is followed by a gradual buildup of an entirely emissive spectrum reaching maximum signal intensity at Δt = 100 μs to match the $T(^{3}P)$, with a resonance profile that is similar to the entirely negative spectrum obtained with continuous illumination. In the R26 carotenoid-less mutant, maximum intensity was observed at Δt = 0 μs, no sign inversion occurred and the pattern of the light induced signals

in the aromatic region was similar to the spectral response observed with continuous illumination. In both WT and R26 maximum signal intensities for the aliphatic carbons are observed with NMR detection immediately following the laser pulse, *i.e.* with Δt = 0 µs (Daviso *et al.* 2010). These signals quickly diminish below the noise level upon increasing the Δt, which was attributed to polarization with opposite sign generated via recombination of the radical pair through the triplet branch versus recombination through the singlet branch (Poleneova and MCDermott, 1999). Based on experimental data and computational analysis, it was put forward that a predominant TSM contribution leads to the observation of emissive photo-CIDNP signals while a predominant DD contribution results in the observation of absorptive signals (Jeschke and Matysik, 2003; Daviso, 2008). In systems with a long living donor triplet, *e.g.* R26 mutants and PSII, an active DR mechanism will cause sign inversion of signals originating from the donor (Prakash *et al.*, 2006). On the other hand significant back transfer from a long living ^{3}P state into the radical pair will result in an inversion of both the donor and the acceptor signals (Chidsey *et al.*, 1985; de Winter and Boxer, 2003; Daviso, 2008 page 19).

Time-resolved photo-CIDNP experiments have not yet been reported for PSI and PSII. In this chapter we present time-resolved photo-CIDNP data obtained from uniformly ^{15}N and selectively 4-ALA ^{13}C labeled PSI and from PSII with ^{13}C at natural abundance, in order to study the mechanism of photo-CIDNP buildup prior to spin diffusion and the electronic structure of the active cofactors in PSI and PSII.

5.2 MATERIALS AND METHODS

5.2.1 Preparation of uniformly ^{15}N- and selectively ^{13}C labeled PSI and natural abundance PSII particles.

Uniformly ^{15}N labeled duckweed plants were grown under aseptic conditions on half-strength Hunter's medium (Posner 1967) with continuous illumination (20 µEm^{-2}s^{-1}) at 25 °C, as described in chapter 3 of this thesis (section 3.2.1). To provide a source of isotope labeled nitrogen, the KNO_3 in the medium was substituted by 5.5 mM of $^{15}NH_4{}^{15}NO_3$, and in addition $Ca(NO_3)\bullet 4H_2O$ was replaced by 4 mM $CaCl_2$. After 7 days plants were harvested, frozen in liquid nitrogen and stored at -80 °C until use. For selective ^{13}C labeling fully grown plants were exposed to 4-ALA δ-aminolevulinic acid (Cambridge Isotope Laboratories), isotopically ^{13}C labeled at carbon position 4. The labeled precursor was added in steps to a

final concentration of 1.4 mM in half-strength Hunter's medium at pH 4.8. After 7 days plants were harvested, frozen in liquid nitrogen and stored at -80 °C until further use. The PSI complex containing ~110 Chl/P700 (PSI-110 particles) was prepared according to the method described by Alia *et al.* 2004. Isolated D1D2 particles from duckweed plants with ^{13}C and ^{15}N at natural abundance were prepared as described earlier in Matysik *et al.* (Matysik 2000).

5.2.2 Time-resolved ns-flash photo-CIDNP MAS NMR experiments

The ns-flash photo-CIDNP MAS NMR experiments were performed with a DMX-200 or a DMX-400 NMR spectrometer (Bruker Biospin GmbH, Karlsruhe, Germany). The NMR probehead was coupled to a Nd:YAG laser (SpectraPhysics Quanta-Ray INDO 40-10, Irvine CA, USA) producing 532-nm laser flashes with an energy between 20 and 270 mJ at 1-4 Hz. For the current study laser flashes with an energy of 200 mJ have been applied. The electronic and optical coupling of the NMR probe with the laser, and the pulse sequence employed in time-resolved photo-CIDNP MAS NMR, are described in detail elsewhere (Daviso 2008). Laser flashes with a duration of ~8 ns were applied, and were separated by a variable evolution period Δt from the NMR $\pi/2$ detection pulse. After each repetitive cycle the residual polarization was erased with an NMR presaturation pulse sequence (Daviso *et al.* 2008b). All data reported in this chapter were obtained at a sample temperature of 235 K and with a spinning frequency of 8 kHz.

5.3 RESULTS AND DISCUSSION

5.3.1 Time-resolved photo-CIDNP experiments on uniformly ^{15}N labeled PSI

Figure 5.3 (see page 93), shows spectra obtained from uniformly ^{15}N labeled PSI-110 particles of duckweed collected with ns laser flashes and with Δt = 0, 10, 100 and 1000 µs (Figure 5.3A, black, green, orange and pink trace respectively). In addition, a spectrum recorded with continuous illumination is shown (Figure 5.3B). A principle difference between the time-resolved spectra in Figure 5.3A and the data obtained with continuous illumination in Figure 5.3B, is a sign inversion for the N-IV signals observed at 247.8, 250.1 and 253.0 ppm, and the N-III signal at 193.3 ppm. The N-II signal occurring at 206.3 ppm in trace B is not visible in trace A.

Table 5.1: ^{15}N chemical shifts for resonances observed by time-resolved photo-CIDNP MAS NMR. Data were obtained from uniformly ^{15}N labeled PSI from duckweed at 4.7 T with Δt = 0 µs, and are compared with literature values from steady state photo-CIDNP experiments and chemical shift predictions by quantum chemical calculations.

Chemical shifts						
Chl *a*	assignment atom	P_B	P_A	A_{0B}	A_0	A_{0A}
σ_{LS}[a]		σ_{SS}	σ_{SS}	σ_{SS}	σ_{SS}	σ_{SS}
186.0	N-I	**186.3 a**	**184.0 a**		**188.6 a**	
		195.6	*193.3*	*196.3*		*192.7*
206.5	N-II	**211.4 e**	**-**		**210.0 a**	
		210.0	*212.1*	*208.3*		*207.3*
189.4	N-III	**191.0 e**	**193.3 e**		**195.7 e**	
		196.9	*198.9*	*193.2*		*194.0*
247.0	N-IV	**254.3 e**	**250.1 a**		**247.8 a**	
		263.2	*255.5*	*252.1*	**253.0 a**	*248.3*
	His-N_τ	**225.4 a**	**-**			
		231.3	*239.5*			

[a] Boxer *et al.* (1974), data obtained in the liquid state from Chl *a* dissolved in $CDCL_3$. Abbreviations: σ, chemical shift, a, absorptive signal, e, emissive signal, LS liquid state, SS solid state. Bold printed chemical shifts represent experimental data, while italic printed chemical shifts are from quantum chemistry calculations (see Apendix B).

Quantum chemical calculations using a triple-zeta basis set and the SAOP model potential were performed to calculate the chemical shifts and ρ_i for the active cofactors in PSI (performed by Bela Bode, see Appendix B). Table 5.1 shows a tentative assignment of the ^{15}N photo-CIDNP signals obtained by time-resolved photo-CIDNP experiments on PSI in a magnetic field of 4.7 T and with Δt = 0 µs (Figure 5.3A, black trace). The assignment is based on the chemical shifts predicted by the calculations, printed in italic in Table 5.1. According to the calculations the cation is mainly localized on the P_B, which is in line with earlier QM/MM calculations and EPR and ENDOR experiments (Käss *et al.* 2001, Saito and Ishikita 2011).

The Mg^{2+} ions of the P_A and P_B cofactors are coordinated to respectively the His residues 680 and 660 of the protein backbone. The quantum chemical modeling predicts that part of the ρ_i is on the imidazole side chain of the histidine residue His680 that is in close proximity to the P_B donor. The chemical shift for the His-N_τ in the calculations is 231.3 ppm (see Table 5.1 and Appendix B). The signal appearing at 225.4 ppm in the datasets obtained from duckweed PSI with Δt = 0 (Figure 5.3A, black trace), is tentatively assigned to the His-N_τ that is coordinated to the Mg of P_B. The 225.4 ppm signal is not visible in the spectra obtained by continuous illumination of the PSI complex from duckweed (Figure 5.3B), while it has been observed earlier in photo-CIDNP MAS NMR data obtained by continuous

illumination of spinach PSI complex, when a short cycle delay of 0.4 s was applied (Diller *et al.* 2007).

The calculations predict mostly emissive signals for the ^{15}N nuclei of P_B and P_A after a single photocycle, except if a negative exchange coupling or unusually long triplet lifetimes were assumed. In line with the relatively short triplet lifetime of T_{3D} ~ 3 µs determined experimentally (Polm and Brettel 1998), mostly emissive photo-CIDNP signals are observed (Figure 5.3A). In addition to the emissive signals, absorptive signals of relatively weak intensity occur at 250.1, ~247, 225.4, 210.0, 188.6 and 186.3 ppm. According to the calculations, TSM leads to a pure emissive spectrum the DD mechanism would give rise to both emissive and absorptive signals. Since both absorptive and emissive signals are observed in the data presented in Figure 5.3A (black trace) the polarization buildup is in line with a dominant DD mechanism. The absorptive signals at 250.1, ~247, 225,4 and 186.3 ppm, have a maximum intensity at Δt = 0 µs (Figure 5.3, black trace) and disappear gradually upon increasing the Δt to 10 µs (Figure 5.3A, green trace) or 100 µs (signal at 188.6 ppm, Figure 5.3A, orange trace). The only exception is the absorptive signal observed at 210.0 ppm, which is present in both the time-resolved and the continuous illumination spectra and increases in intensity upon prolonging the delay time from 0 µs (Figure 5.3A, black trace) to 1 ms (Figure 5.3A, pink trace). The enhanced absorptive signals observed at Δt = 0 can be attributed to a fast decay of the radical pair via the singlet branch, which occurs at the ns timescale. The signal disappears due to the buildup of nuclear polarization with an opposite sign via the triplet branch upon increasing the Δt (see Figure 5.1). In contrast with the pure absorptive spectrum at Δt = 0 µs that was observed for the WT bacterial RC, the spectrum obtained from duckweed PSI shows strong emissive signals for Δt = 0 µs. In addition both absorptive and negative signals decrease in intensity upon increasing the delay time. This can be explained by the the triplet lifetime of $^3[P700^{+\bullet}A_0^{-\bullet}]$, which has been determined to be T_T ~3 µs (Polm and Brettel 1998). This is much shorter than the decay via the carotenoid triplet for the WT bacterial RC, which takes T_{3D} ~10 µs (see Figure 5.2B). Due to the short donor triplet lifetime in combination with the limited time resolution due to the finite NMR $\pi/2$ pulse length of 5 µs, both the polarization associated with the initial non-stationary $^1(D^{+\bullet}A^{-\bullet})$ singlet radical pair state and and the response due to the population of the $^3(D^{+\bullet}A^{-\bullet})$ triplet radical pair generated by the coherent evolution can be observed in the spectra obtained with Δt = 0 and only a residual excess of polarization associated with decay via the $^1(D^{+\bullet}A^{-\bullet})$ singlet radical pair state can be expected.

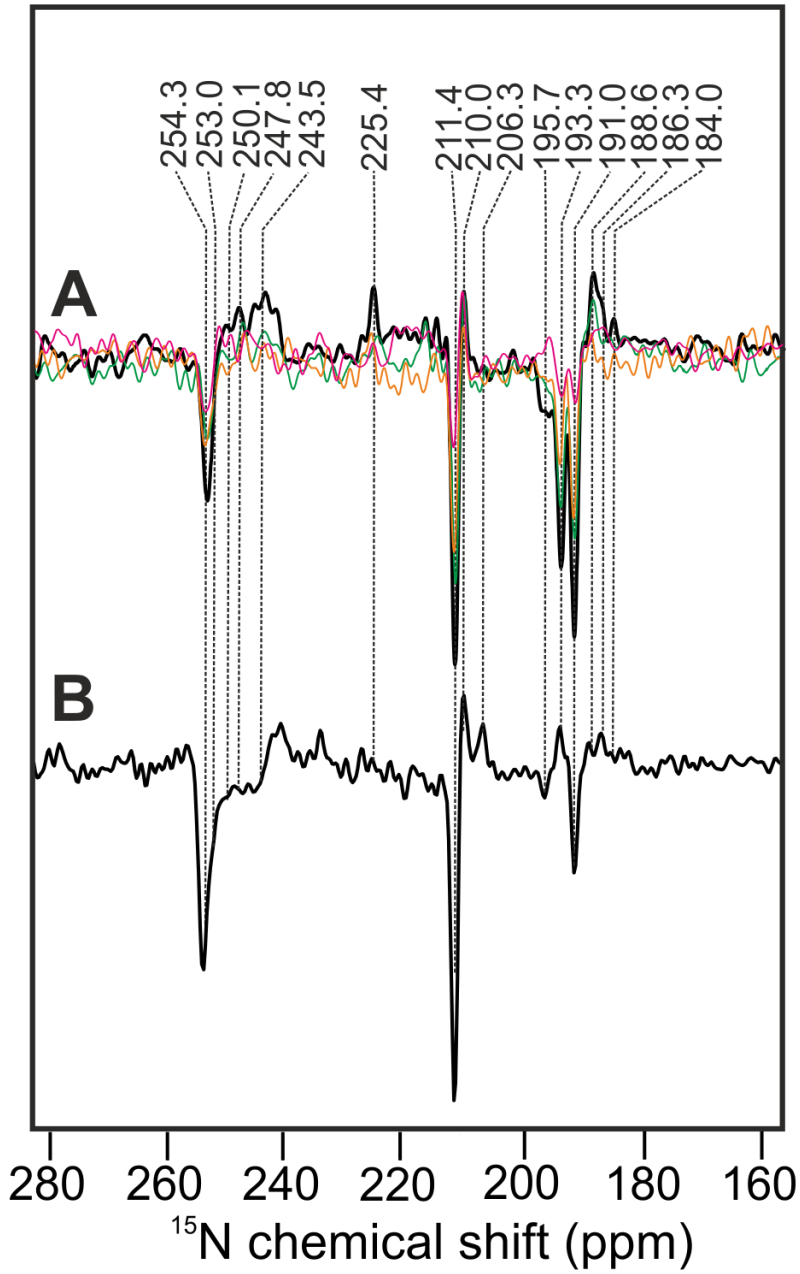

Figure 5.3: ^{15}N-photo-CIDNP MAS NMR spectra obtained from ^{15}N labelled duckweed PSI by ns-flash photo-CIDNP NMR with Δt = 0 µs (A, black trace), Δt = 10 µs (A, green trace), Δt = 100 µs (A, orange trace), Δt = 1 ms (A, pink trace) and by continuous illumination (B) of uniformly ^{15}N labeled PSI-110 particles of duckweed in a magnetic field of 4.7 T and at a temperature of 235K. For the continuous illumination experiments a recycle delay of 4 s was applied.

Upon prolonging the delay time to Δt = 1 ms, no further sign inversion was observed and the changes in relative intensity are small. For 100 µs < Δt < 1 ms (Figure 5.3, orange and pink trace, respectively), the response is different from the steady-state illumination spectrum. This contrasts with the time-resolved photo-CIDNP responses observed for the bacterial RC and for PSII. For these two systems there is apparently a good match between the time-resolved data at longer Δt and the response obtained by continuous illumination

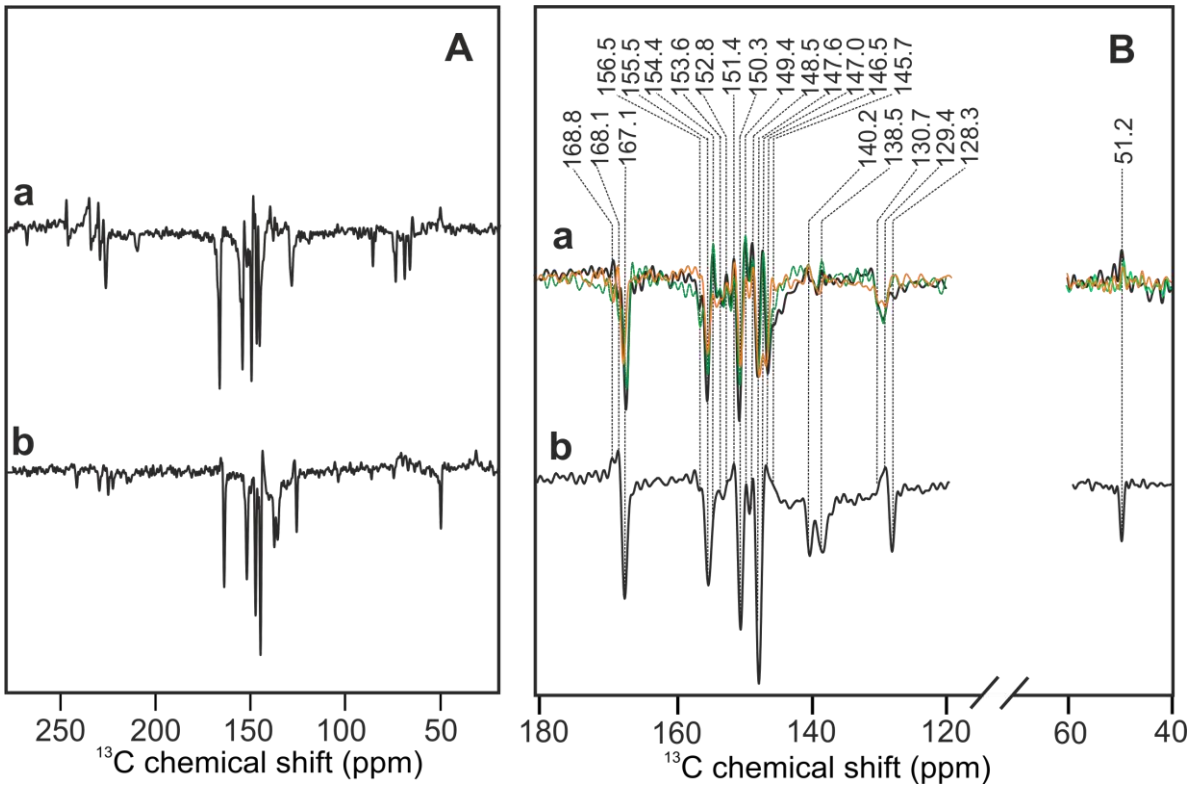

Figure 5.4: (A) ^{13}C photo-CIDNP MAS NMR spectra obtained by laser flash illumination with Δt = 0 µs (a, black trace) and by continuous illumination (b) of 4-ALA labeled PSI particles of duckweed. The signals occurring above 200 ppm and between 55 and 80 ppm are spinning sidebands. Figure B shows the aromatic and aliphatic regions of spectra a and b in A, with the dashed lines indicating the centerbands of the light induced signals. In addition the spectra collected with Δt = 10 µs (green trace) and Δt = 100 µs (orange trace) are depicted. The datasets were collected at a magnetic field strength of 9.4 T, with a recycle delay of 4 s, and using a spinning frequency of 8 kHz.

(Daviso *et al.* 2010 and Figure 5.6). A possible explanation could be that the high energy laser pulses induce trapping of the PSI system in a different state than for continuous illumination. The photo-CIDNP spectrum obtained by continuous illumination shows absorptive signals, while sign inversion is observed for signals associated with both the donor and acceptor upon comparison of the data obtained by continuous illumination. Hence the time-resolved data obatained with Δt = 0 could imply a long lived ^{3}D state. This provides additional support for the high functional flexibility of PSI discussed in chapters 3 and 6.

5.3.2 Time-resolved photo-CIDNP experiments on 4-ALA ^{13}C labeled PSI

Figure 5.4 shows spectra obtained from 4-ALA ^{13}C labeled PSI-110 particles of duckweed collected with ns-laser flashes with Δt = 0 µs (Figure 5.4a), and with continuous illumination (Figure 5.4b). The absorptive signals at 154.4, 152.8, 149.4, 148.5, 147.6, 140.2, 138.5, 128.5 and 51.2 ppm are more pronounced in the dataset obtained with time-resolved

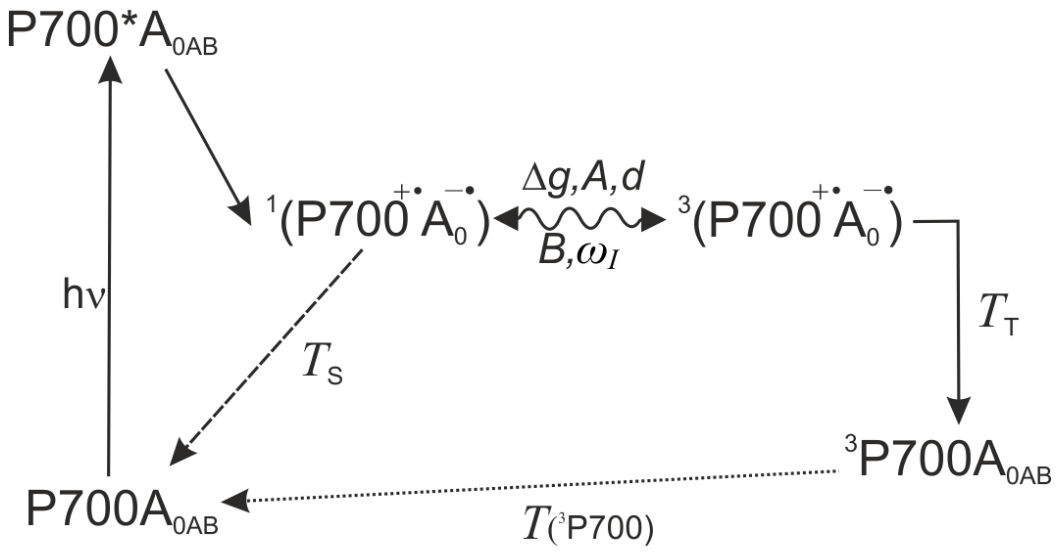

Figure 5.5: Reaction cycle in PSI with reduced F_X and bidirectional electron transfer over both the A and B cofactor branch. After absorption of a photon, ET occurs from the P700 donor to the primary acceptor A_0. Upon reduction of F_X the singlet radical pair lifetime (T_S) increases and the initial pure singlet states are converted into triplet radical pairs and back by coherent evolution. This leads to hyperpolarization of the nuclear states in a complex process, which occurs due to the difference of the *g* values between the two electrons, Δg, the secular part of the hyperfine interaction, *A*, the coupling between the two electrons, *d*, the pseudo-secular hyperfine coupling, *B*, and the nuclear Zeeman frequency, ω_I. The direction of the excitation and decay after light induced electron transfer from the P700 donor to the A_{0A} and A_{0B} Chl *a* acceptors of respectively the A and B cofactor branch, are shown in solid arrows. The radical pair generated upon illumination in PSI decays via the singlet or triplet branch back to the groundstate ($P700A_{0AB}$) with a triplet lifetime, $T_{(^3P700)}$ ~3 µs (Polm and Brettel 1998).

photo-CIDNP at Δt = 0 µs, compared to the same signals in the data that were collected with continuous illumination. In addition, the signals observed with 168.1, 146.5, 145.7, 130.7 and 129.4 ppm chemical shift are emissive in the time-resolved response (Figure 5.4Ba), and absorptive in the spectrum obtained by continuous illumination (Figure 5.4b). When the delay time between the laser pulse and NMR detection is increased to Δt = 10 µs and Δt = 100 µs, the emissive signals at 167.1, 150.3 and 155.5 ppm decrease in intensity. A similar trend is observed for the absorptive signal occurring at 148.5 ppm. It can be observed in the datasets with Δt = 0 µs and Δt = 10 µs, while for the dataset collected with the longer Δt = 100 µs there is no evidence for this response (Figure 5.4A, black, green and orange trace respectively). The aliphatic signal at 51.2 ppm decreases below the noise level for the datasets collected with Δt = 10 and 100 µs.

Based on the quantum chemical shift calculations using a triple-zeta basis set and the SAOP model potential in Appendix B, the response between 167.1 and 168.8 ppm is attributed to the C-19 of the Chl *a*. According to the calculations, the cation is mainly localized on the P_B, which is in line with previous QM/MM calculations and EPR and

ENDOR experiments (Davis *et al.* 1993; Käss *et al.* 2001, Saito and Ishikita 2011). Based on our calculations the response that appears most upfield at 168.8 ppm and has the strongest signal intensity in comparison to the other signals appearing in the C-19 region, is assigned to the P_B cofactor (Figure 5.4B and Appendix B).

The signal arising at 147.0 ppm appears as an absorptive signal of moderate intensity at Δt = 0 and Δt = 10 µs, while it appears as a strong emissive peak at Δt = 100 µs (Figure 5.4Ba) or when continuous illumination is applied (Figure 5.4b). Based on the quantum chemical calculations this signal is tentatively assigned to the C-8 of the P_A or P_B cofactor (see Appendix B). Yet due to the large signal overlap, especially in the region between 140 and 160 ppm and the high functional flexibility of PSI, it is difficult to arrive at a definite assignment of the NMR response at this point. Also the differences between the chemical shifts predicted for the three Chl *a* cofactors (P_B, A_{0A} and A_{0B}) and the one Chl *a*' cofactor (P_A) by calculations are very small (see Appendix B). 2-D and 3-D NMR experiments are proposed in chapter 6 to arrive at a conclusive signal assignment and determine the relative activity in electron transfer for the two cofactor branches in PSI.

Figure 5.5 shows a schematic representation of the spin dynamics of the electron transport in PSI. Both the primary ($P700^{+\bullet}A_0^{-\bullet}$) and subsequently the secondary ($P700^{+\bullet}A_1^{-\bullet}$) radical pair contribute to $^3P700$ buildup (Polm and Brettel 1998). In addition it has been demonstrated that in PSI both cofactor branches are active in ET (Fairclough *et al.* 2003; Ramesh *et al.* 2004; Poluektov *et al.* 2005; Santabarbara *et al.* 2005; Santabarbara *et al.* 2010). This increases the number of radical pairs that can contribute to P700 triplet buildup to four: $P700^{+\bullet}A_{0A}^{-\bullet}$, $P700^{+\bullet}A_{1A}^{-\bullet}$ $P700^{+\bullet}A_{0B}^{-\bullet}$, and $P700^{+\bullet}A_{1B}^{-\bullet}$. However due to the relative large distance between the P700 and the secondary acceptors A_{1A} and $A_{1B,}$ only the primary radical pairs, $P700^{+\bullet}A_{0A}^{-\bullet}$ and $P700^{+\bullet}A_{0B}^{-\bullet}$, are expected to occur at the magnetic field strengths of 4.7 and 9.4 T employed in the current study (Jeschke *et al.* 2011; Figure 5.5).

Upon illumination the PSI forms radical pairs with the electron donor P700 as the radical cation and either the Chl *a* cofactor A_{0A} on the A branch or A_{0B} on the B branch as the radical anion. The relative activity of the A and B branch is known to depend on the organism, cyanobacteria or green algae and plants, and the reduction state of the quinone A_{1A} (Ali *et al.* 2006). In cyanobacteria the relative activity of the B-branch is only 30% while in algae and green plants the activity of the A and B branches are about equal. However upon photo-accumulation of A_{1A}^- after the complete reduction of the F_X cluster, the relative

contribution of the B branch increases and becomes dominant (Santabarbara *et al.* 2006). This will be discussed further in chapter 6.

Reduction of the tightly bound phylloquinones in PSI is much less straightforward than the reduction of the quinones in PSII, which are promptly reduced upon the addition of the chemical reductant dithionite in the dark (Brettel and Golbeck 1995; Rigby *et al.* 1996; Kandrashkin and van der Est 2004; Karyagina *et al.* 2007). Upon dithionite incubation of PSI in the dark only the F_A and F_B clusters are partly reduced, 5 min of subsequent illumination at 205 K reduces the major part of the F_X clusters. When the temperature is increased, a longer photo-accumulation time is required to obtain a similarly large fraction of reduced F_X, *e.g.* a 200% increase of illumination time is required at 220 K (Santabarbara *et al.* 2006). Reduction of F_X causes the formation of the $P700^{+\bullet}A_1^{-\bullet}$ radical pair. Upon prolonged illumination at a high pH of 8 to 10.5, eventually all F_X will reduce. When F_X is reduced, forward ET past A_1 is blocked, which leads to the photo-accumulation of A_1^- and eventually A_0^-. It is suggested that the conditions during our photo-CIDNP experiments result in a relative slow reduction of the F_X cluster due to the relatively high temperature (235 K) and a pH of 9.5. Thus in the initial phase of the photo-CIDNP experiment the F_X will gradually become reduced, resulting in an increasing fraction of the $P700^{+\bullet}A_0^{-\bullet}$ radical pair, which evolves by coherent evolution of the electron-electron zero quantum coherence to the triplet radical and recombines to the $^3P700$ A_0 triplet (see Figure 5.5) allowing photo-CIDNP buildup. The change in the relative contribution of the A and B branch in ET and the changing fraction of reduced F_X, cause additional kinetic effects in the observed photo-CIDNP buildup in PSI, which complicates the interpretation. Due to the high similarity in the environment of the A_{0A} and A_{0B} cofactors and the minimal chemical shift dispersion of the ^{13}C signals, 2D NMR experiments will be required to visualize the relative participation of the two branches in ET (see chapter 6, section 5).

5.3.3 Time-resolved ^{13}C photo-CIDNP MAS NMR experiments on PSII

Spectrum B in figure 5.6 was measured with continuous illumination of PSII D1D2 particles from spinach. Figure 5.6A shows the polarization for the same sample at Δt = 0 µs, obtained by ns laser flash photo-CIDNP. Both spectra are very similar and for longer evolution time Δt = 10 µs and Δt = 1 ms (Figure 5.6A, black, green and pink trace respectively), no sign inversion was observed and changes in the signal pattern in the aromatic region remain

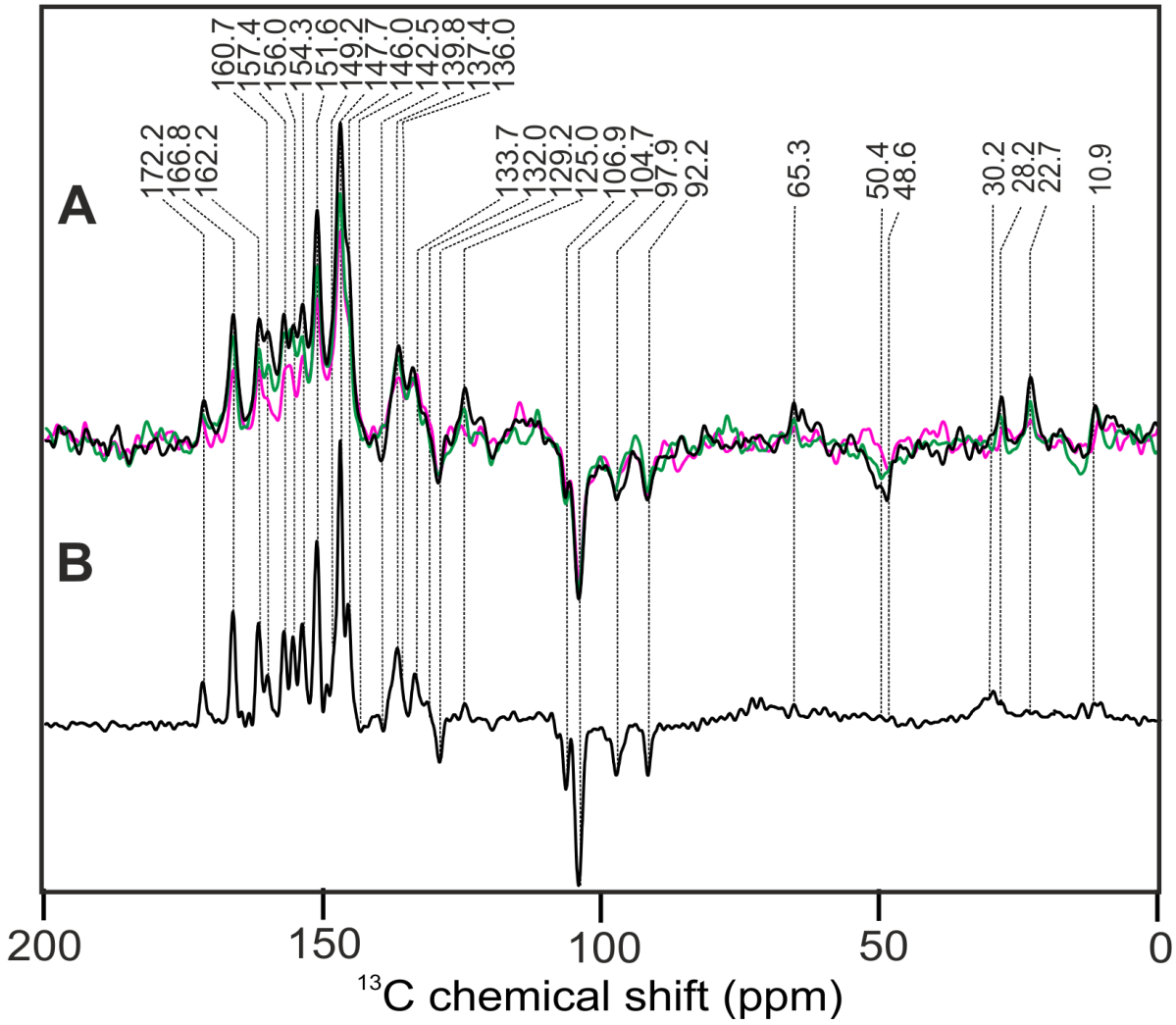

Figure 5.6: ^{13}C photo-CIDNP MAS NMR spectra collected from natural abundance D1D2 PSII particles of spinach with ns-flash photo-CIDNP NMR and (A) a Δt = 0 µs, black trace; Δt = 10 µs, green trace, and Δt = 1 ms, pink trace. The spectrum obtained by continuous illumination is shown in trace B. The data were collected in a magnetic field of 4.7 T and at a temperature of 235 K. Assigned MAS centerband signals are indicated with dashed vertical lines.

within the noise level. Maximum signal intensity was obtained at Δt = 0 µs, with the intensity of all signals decreasing upon prolonged evolution. The aliphatic carbons appear in the continuous illumination spectrum as broad signals of low intensity at 10 and 30 ppm (5.6B). Yet at Δt = 0 µs they are highly resolved and at maximum intensity (Figure 5.6B black trace) after which they disappear upon increasing the delay to 1 ms (Figure 5.6A).

The kinetic scheme of photo-CIDNP buildup in PSII systems was resolved in chapter 4 and is summarized in Figure 5.7. In PSII the negative polarization associated with the ($^3P_{D1}Phe_{D1}$) triplet is fully erased by the DR mechanism for the aromatic carbons at the (P_{D1}) donor side due to paramagnetic longitudinal relaxation occurring during the long lifetime of the ($^3P_{D1}Phe_{D1}$) triplet. Since the anisotropy for the aliphatic carbons is negligible,

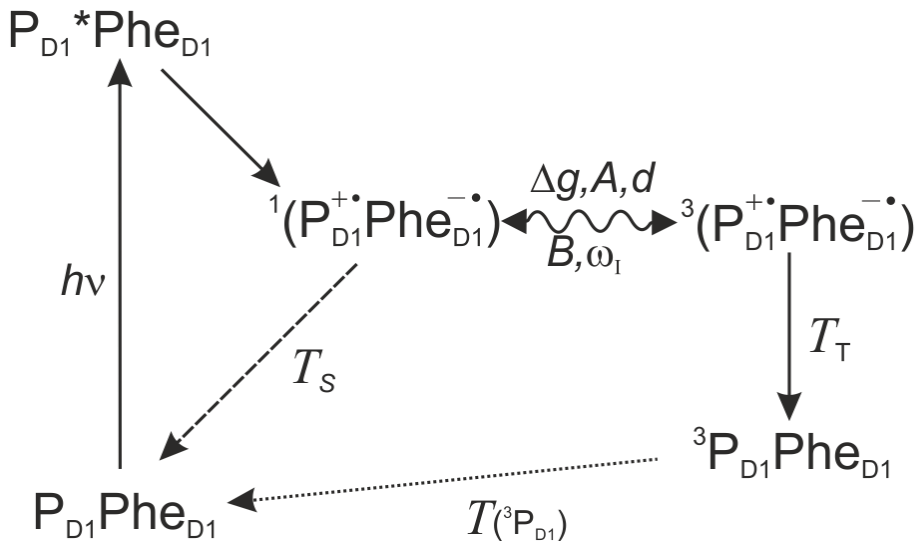

Figure. 5.7: Kinetics and spin dynamics of electron transport for quinone blocked PSII systems and for D1D2 preparations lacking both quinones. Upon removal or double reduction of Q_A the lifetime of the singlet radical pair $P_{D1}^{+\bullet}$ $Phe_{D1}^{-\bullet}$ increases from 20 ns to 250 ns allowing for coherent evolution to the triplet state and photo-CIDNP build-up by the TSM, DD and DR mechanisms.

the contributions from the TSM and DD mechanisms to net polarization buildup and the paramagnetic relaxation (DR) are very weak. The transient observation of the aliphatic signals that are visible at Δt = 0 µs is due to the fast (T_S ~ 250 ns) recombination of the singlet radical pair to the ground state during the NMR detection pulse. The lifetime of the triplet excited state in PSII is 1-3 ms (Hillmann *et al.* 1995; van Mieghem *et al.* 1995), which is considerably longer than the 100 µs found in R26 RCs (Daviso et al. 2009). Therefore the signals in the aliphatic region are gradually quenched by decay via the triplet branch upon increasing the Δt to 1 ms (Figure 5.6A, pink trace).

5.3.4 Conclusions and outlook

In this chapter the first time-resolved photo-CIDNP data from PSI has been presented, by applying ns- laser flash photo-CIDNP MAS NMR to uniformly ^{15}N and 4-ALA ^{13}C labeled PSI. The results suggest that the DD mechanism is the dominant mechanism of photo-CIDNP buildup in PSI. Furthermore the results are in agreement with bidirectional electron transfer and suggest that functional heterogeneity of PSI is an inherent property of PSI. This will be further discussed in chapter 6. To fully elucidate the photo-CIDNP buildup in PSI, where the four cofactors involved in primary ET resonate at similar chemical shift values, 2D and 3D experimentation are proposed in chapter 6. The kinetic effect caused by an increasing fraction of reduced F_X during the photo-CIDNP experiments and the

subsequent change in the relative activity of the A and B branch in ET have to be quantified. To eludiate this, extensive and systematic experimentation on freshly reduced PSI complex preparations by time-resolved photo-CIDNP will be required. The results obtained from D1D2 particles from spinach with ^{13}C at natural abundance reveal a photo-CIDNP buildup in PSII that resembles the buildup observed for *Rb. sphaeroides* R26 RCs. This is attributed to the relatively long triplet lifetime of 1 ms in PSII and 100 μs in R26, which contrasts with the short $T_{(^3D)}$ of 3 μs and 100 ns for the PSI and for *Rb. sphaeroides* WT RCs, respectively. In the next chapter possibilities for the application of ns laser flash photo CIDNP MAS NMR to labeled PSII will be discussed.